Origami tubes assembled into stiff, yet reconfigurable structures and metamaterials

Evgueni T. Filipov[a], Tomohiro Tachi[b], and Glaucio H. Paulino[a,c,1]

[a]Department of Civil and Environmental Engineering, University of Illinois at Urbana–Champaign, Urbana, IL 61801; [b]Graduate School of Arts and Sciences, University of Tokyo, Tokyo 153-8902, Japan; and [c]School of Civil and Environmental Engineering, Georgia Institute of Technology, Atlanta, GA 30332

Edited by David A. Weitz, Harvard University, Cambridge, MA, and approved August 7, 2015 (received for review May 14, 2015)

Thin sheets have long been known to experience an increase in stiffness when they are bent, buckled, or assembled into smaller interlocking structures. We introduce a unique orientation for coupling rigidly foldable origami tubes in a "zipper" fashion that substantially increases the system stiffness and permits only one flexible deformation mode through which the structure can deploy. The flexible deployment of the tubular structures is permitted by localized bending of the origami along prescribed fold lines. All other deformation modes, such as global bending and twisting of the structural system, are substantially stiffer because the tubular assemblages are overconstrained and the thin sheets become engaged in tension and compression. The zipper-coupled tubes yield an unusually large eigenvalue bandgap that represents the unique difference in stiffness between deformation modes. Furthermore, we couple compatible origami tubes into a variety of cellular assemblages that can enhance mechanical characteristics and geometric versatility, leading to a potential design paradigm for structures and metamaterials that can be deployed, stiffened, and tuned. The enhanced mechanical properties, versatility, and adaptivity of these thin sheet systems can provide practical solutions of varying geometric scales in science and engineering.

stiff deployable structures | origami tubes | rigid origami | thin sheet assemblages | reconfigurable metamaterials

Introducing folds into a thin sheet can restrict its boundaries, cause self-interaction, and reduce the effective length for bending and buckling of the material (1–4). These phenomena make thin sheets practical for stiff and lightweight corrugated assemblies (5, 6); however, such systems tend to be static, i.e., functional in only one configuration. For creating dynamic structures, origami has emerged as a practical method in which continuous thin sheet panels (facets) are interconnected by prescribed fold lines (creases). Existing origami patterns and assemblages can easily be deployed; however, they tend to be flexible and need to be braced or locked into a fixed configuration for a high stiffness-to-weight ratio to be achieved (7–10). The zipper-coupled system is different because it is stiff throughout its deployment without having to be locked into a particular configuration.

Origami principles have broad and varied applications, from solar arrays (11) and building façades (12) to robotics (13), mechanisms in stent grafts (14), and DNA-sized boxes (15). The materials and methods used for fabricating, actuating, and assembling these systems can vary greatly with length scale. On the microscale, metallic and polymer films or, more often, layered composites consisting of stiff and flexible materials can be folded by inducing current, heat, or a chemical reaction (16, 17). Large-scale origami structures can be constructed from thickened panels connected by hinges and can be actuated with mechanical forces (11, 18, 19). The kinematic motion, functionality, and mechanical properties of the origami are governed largely by the folding pattern geometry. For example, rigid origami systems are defined as those having a kinematic deformation mode in which movement is concentrated along the fold lines, whereas the panels remain flat (20, 21). Among various rigid folding patterns, the Miura-ori has attracted attention for its folding characteristics (22, 23), elastic stiffness properties beyond rigid folding (24, 25), geometric versatility (26, 27), and intrinsic material-like characteristics (28, 29).

The zipper-coupled tubes introduced here are derived from the Miura-ori pattern and can undergo the same type of rigid kinematic deployment. All other deformations are restrained as they require stretching and shear of the thin sheets. Thus, the structure is light and retains a high stiffness throughout its deployment. It has only one flexible degree of freedom and can be actuated by applying a force at any point (Fig. 1 and Movie S1). To explore unique mechanical properties of the zipper tubes, we introduce concepts of eigenvalue bandgaps and cantilever analyses to the field of origami engineering. Zipper assemblages can be fabricated with a variety of materials and methods. We envision applications of these assemblages will range in size from microscale metamaterials that harness the novel mechanical properties to large-scale deployable systems in engineering and architecture (Movies S2–S4).

This paper is organized as follows. First, the Miura-ori pattern is introduced, and the geometries of three fundamental coupling orientations are discussed. Next, we demonstrate how the system stiffness changes as we assemble two sheets into a tube and then two tubes into the unique zipper-coupled tubes. The fundamental coupling orientations are then studied as deployable cantilevers that can carry perpendicular loads. Next, we discuss cellular assemblages, geometric variations, and practical applications that can be created from coupled tubes, and we conclude with some final remarks.

Geometric Definitions

A Miura-ori cell consists of four equivalent panels, defined by a height a, width c, and vertex angle α (Fig. 2*A*). For our analytical investigation, we use a cell with $a=c=1$ and $\alpha=55°$ as the basis for all structures unless otherwise noted. A sheet is created by repeating this cell $N(=5)$ times in the X direction (Fig. 2*B*). We

Significance

Origami, the ancient art of folding paper, has recently emerged as a method for creating deployable and reconfigurable engineering systems. These systems tend to be flexible because the thin sheets bend and twist easily. We introduce a new method of assembling origami into coupled tubes that can increase the origami stiffness by two orders of magnitude. The new assemblages can deploy through a single flexible motion, but they are substantially stiffer for any other type of bending or twisting movement. This versatility can be used for deployable structures in robotics, aerospace, and architecture. On a smaller scale, assembling thin sheets into these tubular assemblages can create metamaterials that can be deployed, stiffened, and tuned.

Author contributions: E.T.F., T.T., and G.H.P. designed research, performed research, contributed new reagents/analytic tools, analyzed data, and wrote the paper.

The authors declare no conflict of interest.

This article is a PNAS Direct Submission.

See Commentary on page 12234.

[1]To whom correspondence should be addressed. Email: paulino@gatech.edu.

This article contains supporting information online at www.pnas.org/lookup/suppl/doi:10.1073/pnas.1509465112/-/DCSupplemental.

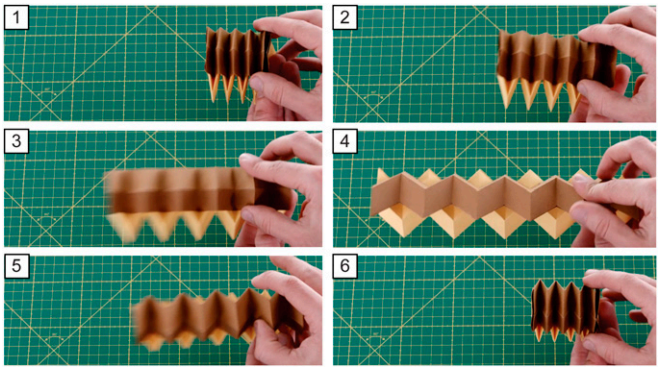

Fig. 1. Deployment and retraction sequence of a zipper-coupled tube system. This origami has only one flexible motion through which it can deform, and thus it is deployed by actuating only on the right end. See Movie S1 for complete simulation.

define the configuration of this sheet as a percentage of extension (a percentage of the maximum extended length $=2Nc$). At 0% extension the sheet lies folded on the $Y-Z$ plane and at 100% extension it lays flat on the $X-Y$ plane. The single tube structure (30) is created by combining the single sheet with its mirrored counterpart (Fig. 2*C* and Movie S5). Previously, Miura-ori sheets and tubes have been coupled (or stacked) to create several different folding assemblages (7, 9, 30, 31). For the zipper orientation of tube coupling, one tube is rotated and connected in a zig-zag (zipper) manner (Fig. 2*D* and Movie S1). We explore the mechanical properties of this assemblage and compare it with an aligned-coupled system where tubes are only translated (30, 31) and an internally coupled system consisting of two compatible tubes (7) (Fig. 2 *E* and *F*). Symmetry in these assemblages permits them to be rigid foldable, meaning that they can fold with no bending of the panels, but only the zipper and aligned systems can reach a flat state when deployed to a 100% extension. The range of extension for internally coupled systems is limited because the internal tube reaches a flat configuration and locks the system in place. Geometric parameters of the compatible internal tube a_I, c_I, and α_I, are discussed in *SI Text*, section S5.

Eigenvalue Analyses

To model the stiffness and mass of origami, we use a bar and hinge approach that provides insight into the structural behavior of the origami assemblages. It captures three fundamental physical behaviors: bending along fold lines, bending of initially flat panels, and stretching and shearing of panels (*SI Text*, section S1 and Fig. S1) (24). The simplicity of the bar and hinge model allows for straightforward implementation and versatility where tubes can be coupled and analyzed as more complex assemblages (see *SI Text*, sections S2 and S5 and Figs. S2 and S3). The model is made scalable and incorporates thickness ($t=0.01$), Young's modulus ($E=10^6$), Poisson's ratio ($\nu=1/4$), and density ($\rho=1$) of the material (32). A parameter, $R_{FP}=1/10$, relates fold line bending to panel bending stiffness and can vary greatly, depending on the materials, the fabrication technique, and the actuation process (33–36). Using a sensitivity analysis in *SI Text*, section S3 and Fig. S4, we show that the value of R_{FP} and other parameters do not affect the qualitative results and conclusions presented in this paper. A finite-element (FE) model, where each panel is discretized with shell elements, is used to verify the results and to study local deformations and stress concentrations in the origami (*SI Text*, section S4; Fig. 3; and Figs. S5–S7). The bar and hinge model cannot capture all localized effects, but it is significantly faster and provides a sufficiently high level of accuracy for global origami behaviors.

Stiffness (**K**) and mass matrices (**M**) are used to construct a linear dynamics system of equations $\mathbf{K}v_i=\lambda_i\mathbf{M}v_i$ (no sum), where λ_i is the ith eigenvalue and v_i is the corresponding eigenmode of the structure. Each eigenmode represents a structural deformation mode of the system, and its corresponding eigenvalue (in units of $1/s^2$) represents an excitation frequency that would result in the given deformation. The eigenvalue is proportional to the total energy in the system (kinetic and elastic strain energy), meaning that a deformation mode with higher energy will require a higher excitation frequency. The structure is analyzed with no boundary constraints, and thus the first six eigenmodes correspond to rigid body motion of the structure in 3D space (three displacement and three rotational modes). We omit these modes from our study, as they require zero energy. The seventh eigenmode and those following represent deformations requiring incremental energy input. The eigenvalues of a single Miura-ori sheet, a single tube, and a zipper-coupled tube are plotted vs. percentage of extension (Fig. 3 *A–C*), and representative deformation modes are shown for each structure at 70% extension (Fig. 3 *D–F*). Eigenvalues scale linearly with mass and stiffness and therefore comparisons remain scale independent and highlight the influence of coupling on the global system behaviors. The single sheet can bend and twist globally in several directions with little energy input, resulting in low eigenvalues. The distribution of energy for the seventh and eighth deformation modes (Fig. 3*G* and Fig. S7) illustrates that bending occurs in the central panels and folds whereas the remainder of the structure remains unstressed. As expected, the bending energy in the panels is highest at the vertices, where the curvature approaches infinity (1, 37). The ninth mode of the sheet and the seventh mode of the tube represent a rigid folding motion where bending is primarily concentrated in the folds and the panels remain essentially flat throughout the deformation (Fig. 3 *D* and *E*).

For practical purposes, we prefer that λ_7 corresponds to rigid folding and that subsequent eigenvalues are higher, creating a bandgap $\beta=\lambda_8-\lambda_7$. A structure with a large bandgap has a

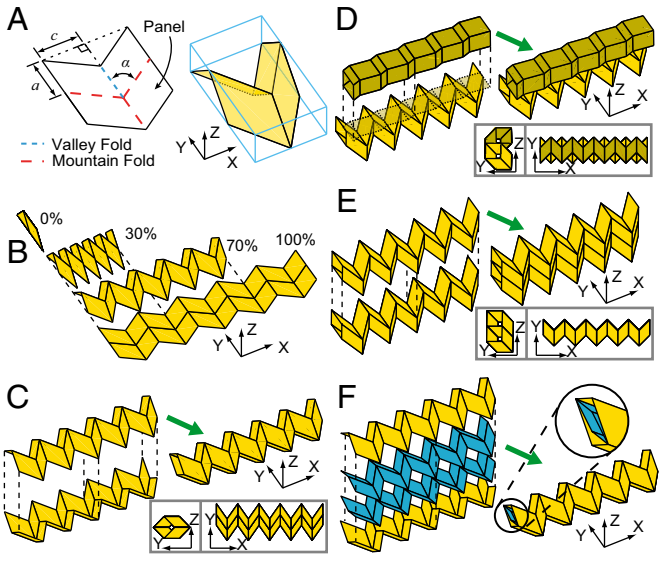

Fig. 2. Geometry and assembly of origami tube structures. (*A*) Miura-ori pattern defined with $a=c=1$, $\alpha=55°$ and folded into a three-dimensional Miura-ori cell. This cell is used as the basis for all structures unless otherwise noted. (*B*) A Miura-ori sheet in four configurations defined as a percentage of extension. (*C*) Two mirror-image sheets shown at 70% extension and combined into a rigid, flat foldable tube. (*D*) Zipper-coupled tubes. A tube is translated and rotated in the $Y-Z$ plane until the opposing faces of the two tubes align. For clarity, a different shade is used for one of the zipper tubes, but both tubes are identical to the definitions in *A–C*. (*E*) Aligned-coupled tubes. A tube is translated in the $Y-Z$ plane and coupled with the tube in the initial configuration. (*F*) Internally coupled tubes, inspired by ref. 7. External tube is the same as in *C*, and the internal tube is defined to reach a flat configuration when the external tube is at 80% extension.

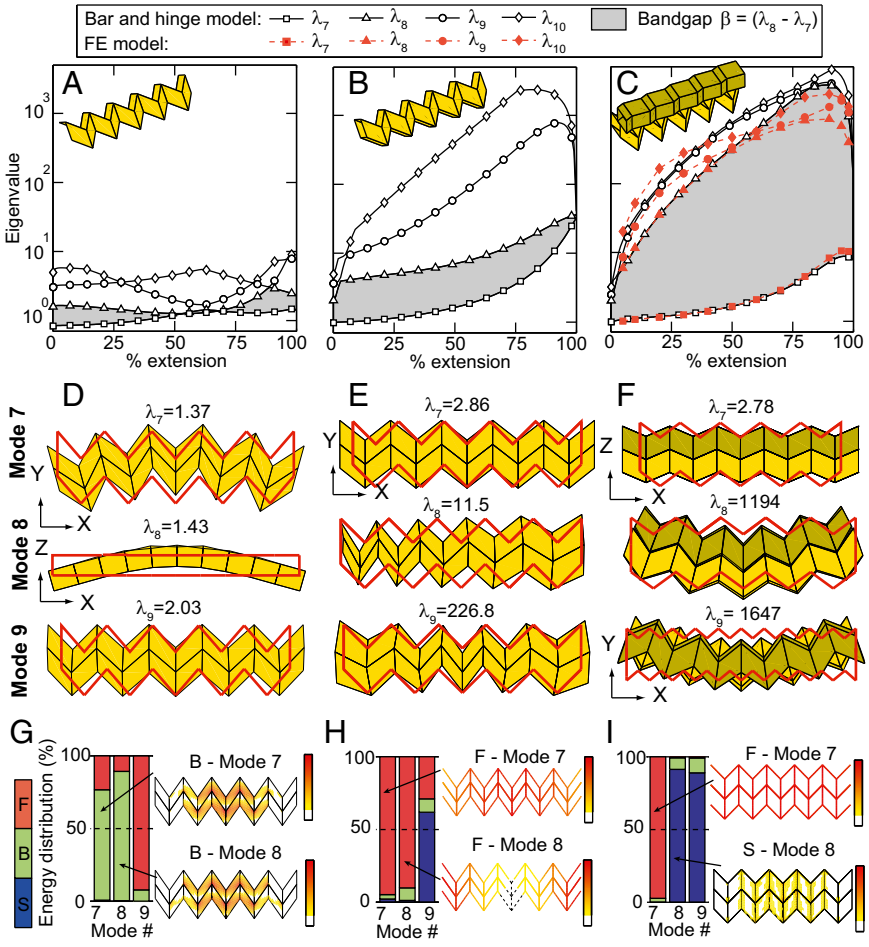

Fig. 3. Stiffness characteristics of a sheet, a single tube, and a zipper-coupled tube. (*A–C*) Eigenvalue vs. configuration (percentage of extension) for the sheet, the single tube, and zipper-coupled tubes, respectively. The large bandgap from the zipper-coupled tubes is also verified with an FE model. (*D–F*) Seventh, eighth, and ninth deformation eigenmodes when structures are at 70% extension (undeformed outline in red). (*G–I*) Energy distributions for the sheet, the single tube, and zipper tubes, respectively. The energy distribution is presented as a bar graph indicating the percentage of energy in fold bending (F), panel bending (B), and panel stretching and shearing (S). Representative element energies are shown for modes 7 and 8 of each structure. For detailed energy presentation see *SI Text*, section S4 and Fig. S7.

flexible mode that allows for easy deployment but is stiff for all other types of loading. Mode switching may occur, meaning that the deformed shape corresponding to a given eigenvalue can differ drastically, depending on extension. For example, the seventh and eighth modes switch for the single Miura-ori sheet around 70% extension (Fig. 3*A*). The single and zipper-coupled tubes display a continuous bandgap and do not experience switching of the rigid folding mode (seventh). The eighth mode of the single tube constitutes a "squeezing" deformation, where one end of the structure is folded and the other end is unfolded (Fig. 3*E* and Movie S5). This mode requires bending of folds and panels at the ends of the structure; however, the panels do not stretch or shear, and thus λ_8 is only slightly higher than λ_7. The aligned and internally coupled assemblages are also prone to squeezing and the bandgap is not increased (*SI Text*, section S5 and Fig. S8).

However, when coupling the tubes into a zipper assemblage we observe that the structure has a substantially increased bandgap, where λ_8 is often two orders of magnitude greater than λ_7. The large increase in λ_8 occurs because all deformation modes except for rigid folding (λ_7) require stretching and shearing of the thin sheets and thus a substantially higher amount of energy. Deforming the zipper-coupled tubes in a global bending mode (eighth or ninth) requires stretching the structure's panels (Fig. 3 *F* and *I*). When actuated at one end, a single, aligned, or internally coupled tube squeezes (Movie S5 and Fig. S8), whereas zipper-coupled tubes expand and contract in a consistent rigid folding motion (Fig. 1 and Movie S1). The zipper-coupled tubes are not prone to the squeezing-type deformation, as it would require differential movement between the tubes and stretching the thin sheet (*SI Text*, section S2 and Fig. S3).

Structural Cantilever Analyses

The zipper, aligned, and internally coupled tube systems can be applicable as deployable cantilever structures when restrained on one end (Fig. 4). At the supported end all nodes are fully fixed (X, Y, and Z displacements), whereas a total load of 1 is distributed on the other end of the structure (Fig. S9 *D–F*). When used as cantilevers, the tubes exhibit behavior similar to that of an I-beam, wherein the second moment of area (or area moment of inertia) is increased by distributing material away from the centroid. The aligned and internally coupled tube systems often experience squeezing-type deformations when loaded on one end, whereas the zipper-coupled tubes experience more uniform bending deformations (Fig. 4*A*). The stiffness of the structures is calculated for the three Cartesian directions for different extensions (Fig. 4 *B–D*). The loads are applied for each configuration, and the resultant displacements (Δ_X, Δ_Y, and Δ_Z) are calculated from the linear function $\mathbf{F}=\mathbf{K}\Delta$, where $\mathbf{F}$ is a force vector. A quantitative stiffness of the system is then calculated as $K=F/\delta=1/\delta$ based on the maximum system displacement (δ). The zipper-coupled tubes tend to be stiffer than the other two systems and have a greater stiffness when closer to full extension. The internally coupled tubes tend to be stiff for Z-direction loading and when locked into a fixed configuration (i.e., 80% extension). The results for stiffness presented here show the general system behavior and are in consistent units of force per length (e.g., newtons per millimeter). A realistic length scale and elastic modulus can be substituted to find quantitative results for the cantilevers.

The stiffness for different directions of loading, orthogonal to the X axis, is investigated, by rotating the load in the $Y-Z$ plane. The stiffness for each structure is calculated at extensions of 40%,

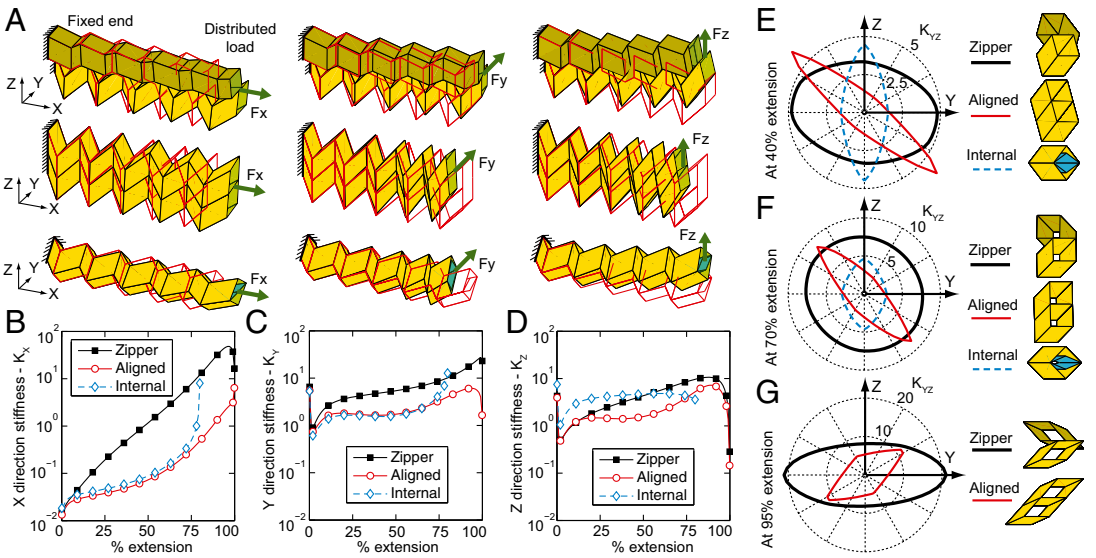

Fig. 4. Zipper, aligned, and internally coupled tubes used as cantilevers. (*A*) Initial (red line) and deformed geometry of the structures at 70% extension when the left end is fixed and a uniform load is applied on the right end. The deformed shapes are scaled so the maximum displacement for each case is equal to the panel height ($a = 1$) and do not necessarily represent stiffness. (*B–D*) The stiffness (force/length) of the cantilevers in the three Cartesian directions. The internally coupled tube cannot extend beyond 80% extension of the external tube. (*E–G*) The stiffness for loads in the $Y-Z$ plane represented as a radial plot at extensions of 40%, 70%, and 95%, respectively. Stiffness is shown as distance from the origin.

70%, and 95% and presented as a radial plot corresponding to the direction of loading (Fig. 4 *E–G*). The structure is analyzed with the same constraint and load distributions, and only the direction of the load vector (equating to 1) is rotated in the $Y-Z$ plane. The aligned and internally coupled tube systems demonstrate anisotropic behavior, wherein only one loading direction (in the $Y-Z$ plane) displays high stiffness. On the other hand, the zipper-coupled tubes tend to be stiff for all directions of loading, as depicted by the more circular profile on the plots (Fig. 4 *E–G*).

The fixed end of the cantilevers may be constrained in a different fashion, so that a mechanism is installed to fold and deploy the entire structure (Fig. S9 *G–I*). The mechanism would control the rigid folding mode of the system, thus permitting easy deployment (especially for zipper-coupled tubes—see actuation in Movie S1). When the mechanism is contracted, the structure will deploy, and when it is extended, the structure will fold. When the length of the mechanism is fixed, the cantilever will behave much as if the support is fully fixed.

Cellular Assemblages

Cellular origami can permit self-assembly of engineered hierarchical materials (5, 38), whose mechanical properties depend on the microstructure geometry. The structural stiffness and energy absorption properties of cellular origami can be optimized to complement and improve naturally occurring materials (39). Zipper-coupled tubes can be integrated with aligned or internal coupling to create layered foldable assemblages (Fig. 5 and Movie S3). Structures that incorporate zipper coupling inherit the large bandgap, while also retaining properties from the other coupling techniques (e.g., space filling from aligned or locking from internal coupling). The zipper/aligned metamaterial studied in Fig. 5 *B–E* has the same parameters as before, except the fold to panel stiffness ratio is set to $R_{FP} = 1$, to simulate an assemblage constructed by additive manufacturing (Fig. 5 *F* and *G*). Origami metamaterials created with 3D printing do not fold like traditional origami, but possess novel characteristics such as the single flexible mode of zipper coupling.

We analyze the assemblage in Fig. 5 by applying symmetric uniform forces (summing to 1) on opposing faces of the system and calculate the compression stiffness as $K = F/\delta = 1/\delta$, where δ is the mean total displacement in the direction of loading. Because of the zipper geometry, the system is primarily flexible in the X direction at lower extensions (0–70%) and in the Y direction at higher extensions (70–100%). The peak in the Y-direction stiffness (at 96.4% extension) corresponds to a bistable state, where the tube cross section is square, and can transition to a different rhombus, depending on the direction of folding (Movie S3). In addition to the stiffness, the deformation characteristics of the material are also anisotropic. The perceived Poisson's ratio is negative in the Y direction when compressed in X, whereas it is positive in the Z direction when compressed in Y (Fig. 5 *C* and *D*). The structure is substantially stiffer in the Z direction, and deformations do not follow the kinematic folding mode.

Geometric Variations

There are numerous other ways in which rigid foldable tubes can be defined, combined, and coupled. For example, a different vertex angle α and panel height a may be used with rigid and flat foldability of the system preserved. Zipper coupling can be continued in one direction to create an easily deployable slab structure resistant to out-of-plane loads; potential applications are architectural canopies (Fig. 6*A*), bridges (Fig. 6*B*), solar arrays, or synthetic materials. When the vertex angle is varied for the coupled zipper tubes, we can create arbitrarily curved systems with high out-of-plane stiffness (Fig. 6*A* and Movie S4). The bridge deck uses tubes with a vertex angle of $\alpha = 85°$ to provide a more even surface, whereas the bridge parapet tubes have a lower vertex angle to provide stiffness during deployment (Fig. 6*B* and Movie S2). If the zipper coupling is repeated in more than one direction, the structure will self-interlock during the deployment, creating a stiff array of coupled thin sheets (Fig. 6*C* and Movie S2). The structure does not necessarily need to have a square final cross section (four segments of zipper-coupled tubes), but can be any radially symmetric shape (*SI Text*, section S6).

The cross section of the tubes is not restricted to a quadrilateral shape (30, 31); any polygon with translational symmetry can be used to extrude a rigid, foldable origami tube. The tubes can have any cross section where each segment of the cross section has an equal-length counterpart (or counterparts) that is (are) translationally symmetric. The internal panels of the six-sided polygonal tube (blue in Fig. 7*A* and Movie S2) are defined to conform with the flat and rigid foldability of the system. The

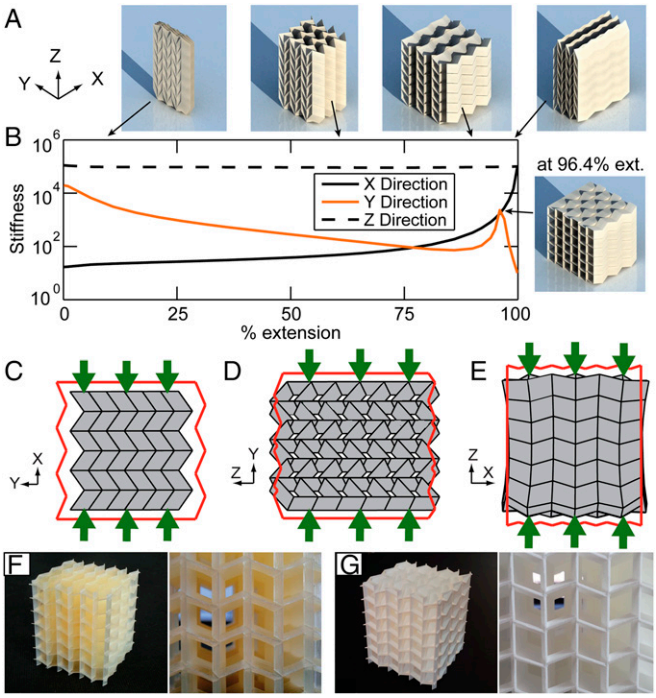

Fig. 5. Cellular origami metamaterial consisting of 36 tubes with $\alpha = 75°$, $N = 3$ arranged as zipper in the horizontal Y direction and as aligned in the vertical Z direction. (*A*) Kinematic folding sequence of the assemblage (Movie S3). (*B*) Compression stiffness of the metamaterial in the three Cartesian directions vs. extension. (*C*–*E*) Initial (red line) and deformed geometry of the assemblage at 90% extension for uniform compression tests in the X, Y, and Z directions, respectively. The deformed shapes are scaled so the mean displacement of the loaded surfaces is equal to the panel height ($a = 1$) and do not represent stiffness. (*F* and *G*) Metamaterial prototypes constructed with additive manufacturing cannot undergo the full folding motion in *A*, but inherit the anisotropic mechanical properties of the cellular zipper assemblages. In *F* a soft metamaterial from resin with a wall thickness of 0.09 mm can be deformed by hand, whereas the polyamide assemblage in *G* with a wall thickness of 0.8 mm is substantially stiffer (*Materials and Methods*).

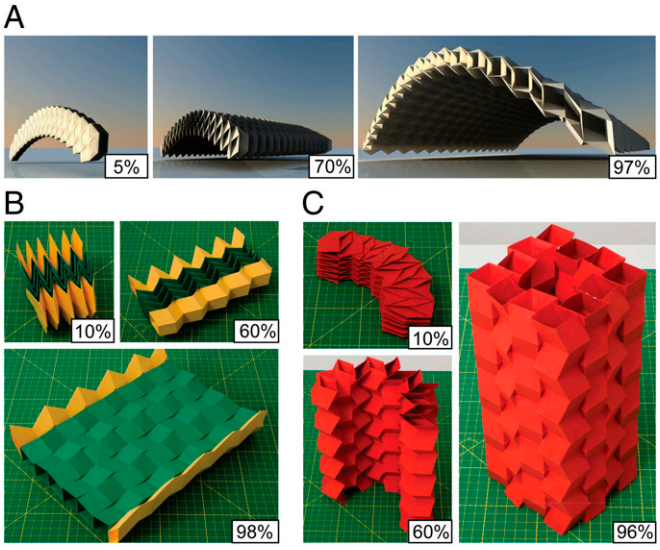

Fig. 6. Variations of cellular assemblages in different stages of deployment. Approximate percentage of extension is shown. (*A*) Deployable architectural canopy with high out-of-plane stiffness for transformable building design. (*B*) Bridge structure from zipper-coupling tubes of different geometries. The structure is flat foldable in two directions and stiff for out-of-plane loading. (*C*) Structure that interlocks into a fully conforming shape. The structure's edges are each composed of four tubes coupled in a zipper orientation. For details see Table S1 and Movie S2.

direction of the folds in these segments can be reversed (e.g., mountain to valley), thus changing the geometry. Polygonal tubes with more sides can be reconfigured in the same way, with many more variable cross sections. In Fig. 7*B* we show that finite thickness may also be incorporated into the construction of the coupled origami tubes. Using available techniques for thick origami (18, 19), we can create structures of thick panels adjoined with physical hinge elements. With these techniques cost-effective materials (e.g., thin wood panels with metal hinges) can be used to create large structures that can be easily deployed, but possess large global stiffness from the zipper-coupling framework. Finally, the characteristics of origami assemblages can be modified by coupling only specific portions of a tube. The long tube in Fig. 7*C* has zipper coupling only in the middle portion to restrict the global squeezing and bending of the system. The ends remain uncoupled, allowing for a rigid connection to the outside edge while still permitting the system to fold and unfold.

Concluding Remarks

This paper introduces an approach for coupling origami tubes in a zipper fashion and explores their unique mechanical characteristics. These assemblages engage the thin sheets in tension, compression, and shear for any deformation mode that does not follow the kinematic deployment sequence. The origami tubes can be stacked and coupled into a variety of cellular assemblages that can further enhance the mechanical characteristics and versatility of the systems. Extensions and refinements of this work may explore geometric arrangements that improve the stiffness-to-weight ratio, and impact energy dissipation and other mechanical properties. Further study of the hierarchical system properties with respect to fabrication, scale, and materials will be needed to inform potential applications. As origami becomes more widely used in science and engineering, the coupled tube assemblages will serve as an important component that allows flexible deployment while simultaneously retaining a high global stiffness.

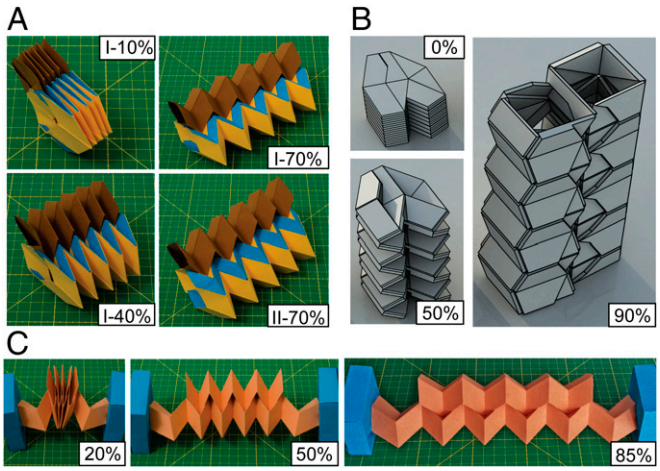

Fig. 7. Local variations in coupling origami tubes. Different stages of deployment are shown with approximate percentage of extension. (*A*) Zipper coupling of a reconfigurable tube with a polygonal cross section. The six-sided polygonal tube has two possible shapes (I and II). (*B*) Computer visualization of zipper tubes from thick material (thick origami). (*C*) Actuator system from zipper coupling of two tubes of different length. The edges of the long tube are restrained, but squeezing can occur on the uncoupled sections, allowing the system to fold. For details see Table S1.

Materials and Methods

Prototypes of the origami were created for demonstrating the mechanical characteristics and for showing the kinematic folding. The origami assemblages in Movies S1, S2, and S5 and Figs. 1, 6, and 7 are created from perforated paper that is folded and adhered together. The Miura-ori sheets were created from 160-g/m^2 paper by perforating along the fold lines with cuts of length 0.5 mm spaced evenly at 1-mm intervals. Because each tube cannot be developed from a single flat piece of paper, it is assembled by connecting two Miura-ori sheets (Fig. 2*C* and Movie S5). One of the sheets is constructed with perforated tabs at the edge, which can be folded and attached with standard paper adhesive to a mirror-image Miura-ori sheet. When connecting two tubes into either the zipper or the aligned assemblage, the adjacent facets are adhered together (Fig. 2 *D* and *E* and Movie S1). For internally coupled tubes, the structure is assembled in sequence (Fig. 2*F*) by connecting individual Miura-ori sheets with the joining tabs. The numerous variations of the coupling configurations (Figs. 6 and 7) were also assembled using the same techniques. In Fig. 5 *F* and *G*, we show how additive manufacturing can be used to create cellular metamaterials with characteristics inherited from the zipper tubes. The model in Fig. 5*F* was created with a Keyence AGILISTA 3000 3D printer that uses digital light processing (DLP) technology. The model material is an AR-M2 transparent resin and the support material is an AR-S1 water-soluble resin. The cube has dimensions of $68 \times 62 \times 61$ mm with wall thickness of 0.09 mm. The model in Fig. 5*G* was created with an EOS Formiga P 100 selective laser sintering (SLS) system. The model uses a PA 2200 (Polyamide 12) material that is sintered together and does not require support material. This assemblage has dimensions of $102 \times 93 \times 92$ mm with wall thickness of 0.8 mm.

ACKNOWLEDGMENTS. This work was partially funded by the National Science Foundation (NSF) through Grant CMMI 1538830. E.T.F. is grateful for support from the NSF Graduate Research Fellowship and the Japan Society for the Promotion of Science Fellowship. The authors also acknowledge support from the Japan Science and Technology Agency Presto program and the Raymond Allen Jones Chair at the Georgia Institute of Technology.

1. Lobkovsky AE, Gentges S, Li H, Morse D, Witten TA (1995) Scaling properties of stretching ridges in a crumpled elastic sheet. *Science* 270(5241):1482–1485.
2. Vliegenthart GA, Gompper G (2006) Forced crumpling of self-avoiding elastic sheets. *Nat Mater* 5(3):216–221.
3. Cambou AD, Menon N (2011) Three-dimensional structure of a sheet crumpled into a ball. *Proc Natl Acad Sci USA* 108(36):14741–14745.
4. Witten TA (2007) Stress focusing in elastic sheets. *Rev Mod Phys* 79(2):643–675.
5. Côté F, Deshpande VS, Fleck NA, Evans AG (2006) The compressive and shear responses of corrugated and diamond lattice materials. *Int J Solids Struct* 43(20): 6220–6242.
6. Yokozeki T, Takeda S, Ogasawara T, Ishikawa T (2006) Mechanical properties of corrugated composites for candidate materials of flexible wing structures. *Compos Part A Appl Sci Manuf* 37(10):1578–1586.
7. Schenk M, Guest SD (2013) Geometry of Miura-folded metamaterials. *Proc Natl Acad Sci USA* 110(9):3276–3281.
8. Heimbs S (2013) Foldcore sandwich structures and their impact behaviour: An overview. *Dynamic Failure of Composite and Sandwich Structures*, eds Abrate S, Castanié B, Rajapakse YDS (Springer, Dordrecht, The Netherlands), Vol 192, pp 491–544.
9. Cheung KC, Tachi T, Calisch S, Miura K (2014) Origami interleaved tube cellular materials. *Smart Mater Struct* 23(9):094012.
10. Gattas JM, You Z (2015) Geometric assembly of rigid-foldable morphing sandwich structures. *Eng Struct* 94:149–159.
11. Zirbel SA, et al. (2013) Accommodating thickness in origami-based deployable arrays. *J Mech Des* 135(11):111005.
12. Del Grosso AE, Basso P (2010) Adaptive building skin structures. *Smart Mater Struct* 19(12):124011.
13. Felton S, Tolley M, Demaine E, Rus D, Wood R (2014) Applied origami. A method for building self-folding machines. *Science* 345(6197):644–646.
14. Kuribayashi K, et al. (2006) Self-deployable origami stent grafts as a biomedical application of Ni-rich TiNi shape memory alloy foil. *Mater Sci Eng A* 419(1–2):131–137.
15. Andersen ES, et al. (2009) Self-assembly of a nanoscale DNA box with a controllable lid. *Nature* 459(7243):73–76.
16. Gracias DH, Kavthekar V, Love JC, Paul KE, Whiteside GM (2002) Fabrication of micrometer-scale, patterned polyhedra by self-assembly. *Adv Mater* 14(3):235–238.
17. Peraza-Hernandez EA, Hartl DJ, Malak RJ, Jr, Lagoudas DC (2014) Origami-inspired active structures: A synthesis and review. *Smart Mater Struct* 23(9):094001.
18. Hoberman C (2010) Folding structures made of thick hinged sheets. US Patent 7,794,019 B2,14.
19. Tachi T (2011) Rigid-foldable thick origami. *Origami 5*, eds Wang-Iverson P, Lang RJ, Yim M (CRC, Boca Raton, FL), pp 253–263.
20. Huffman DA (1976) Curvature and creases: A primer on paper. *IEEE Trans Comput* C-25(10):1010–1019.
21. Hull TC (2012) *Project Origami: Activities for Exploring Mathematics* (CRC, Boca Raton, FL), 2nd Ed.
22. Mahadevan L, Rica S (2005) Self-organized origami. *Science* 307(5716):1740.
23. Miura K (2009) The science of Miura-ori: A review. *Origami 4*, ed Lang RJ (AK Peters, Natick, MA), pp 87–99.
24. Schenk M, Guest SD (2011) Origami folding: A structural engineering approach. *Origami 5*, Wang-Iverson P, Lang RJ, Yim M (CRC, Boca Raton, FL) pp 293–305.
25. Wei ZY, Guo ZV, Dudte L, Liang HY, Mahadevan L (2013) Geometric mechanics of periodic pleated origami. *Phys Rev Lett* 110(21):215501.
26. Tachi T (2009) Generalization of rigid foldable quadrilateral mesh origami. *Proceedings of the International Association for Shell and Spatial Structures*, eds Domingo A, Lazaro C (Universidad Politecnica de Valencia, Valencia, Spain), pp 2287–2294.
27. Gattas JM, Wu W, You Z (2013) Miura-base rigid origami: Parameterizations of first-level derivative and piecewise geometries. *J Mech Des* 135(11):111011.
28. Silverberg JL, et al. (2014) Applied origami. Using origami design principles to fold reprogrammable mechanical metamaterials. *Science* 345(6197):647–650.
29. Lv C, Krishnaraju D, Konjevod G, Yu H, Jiang H (2014) Origami based mechanical metamaterials. *Sci Rep* 4:5979–5981.
30. Tachi T (2009) One-Dof cylindrical deployable structures with rigid quadrilateral panels. *Proceedings of the International Association for Shell and Spatial Structures*, eds Domingo A, Lazaro C (Universidad Politecnica de Valencia, Valencia, Spain), pp 2295–2305.
31. Tachi T, Miura K (2012) Rigid-foldable cylinders and cells. *J Int Assoc Shell and Spatial Structures* 53(4):217–226.
32. Filipov ET, Tachi T, Paulino GH (2015) Toward optimization of stiffness and flexibility of rigid, flat-foldable origami structures. *The 6th International Meeting on Origami in Science, Mathematics and Education*, eds Kawasaki T, Uehara R, Tachi T, Maekawa J (University of Tokyo, Tokyo), p 121.
33. Lauff C, et al. (2014) Differentiating bending from folding in origami engineering using active materials. *Proceedings of the ASME 2014 International Design Engineering Technical Conferences & Computers and Information Engineering Conference* (ASME, Buffalo, NY), p V05BT08A040.
34. Giampieri A, Perego U, Borsari R (2011) A constitutive model for the mechanical response of the folding of creased paperboard. *Int J Solids Struct* 48(16–17):2275–2287.
35. Mentrasti L, Cannella F, Pupilli M, Dai JS (2013) Large bending behavior of creased paperboard. I. Experimental investigations. *Int J Solids Struct* 50(20–21):3089–3096.
36. Lechenault F, Thiria B, Adda-Bedia M (2014) Mechanical response of a creased sheet. *Phys Rev Lett* 112(24):244301.
37. Cerda E, Chaieb S, Melo F, Mahadevan L (1999) Conical dislocations in crumpling. *Nature* 401(6748):46–49.
38. Fratzl P, Weinkamer R (2007) Natures hierarchical materials. *Prog Mater Sci* 52(8): 1263–1334.
39. Gibson LJ, Ashby MF, Harley BA (2010) *Cellular Materials in Nature and Medicine* (Cambridge Univ Press, Cambridge, UK).
40. Ahn BY, et al. (2010) Printed origami structures. *Adv Mater* 22(20):2251–2254.
41. Hibbitt D, Karlsson B, Sorensen P (2010) ABAQUS FEA Version 6.10 (Dassault Systemes, Vélizy-Villacoublay, France).